Analytical Expressions for the Mutual Coupling of Loop Antennas Valid From the RF to Optical Regimes

Jogender Nagar, *Student Member, IEEE*, Bing Qian Lu, *Student Member, IEEE*, Mario F. Pantoja, *Senior Member, IEEE*, and Douglas H. Werner, *Fellow, IEEE*

***Abstract*— Arrays of circular loop antennas are commonly employed at radio frequencies for communications and geophysical sensing, while also holding enormous potential in the optical regime for applications such as solar energy harvesting. Exact analytical expressions exist for predicting the mutual coupling between a variety of antennas, including dipoles and slots. However, due to the complexity of the integrals involved, analytical expressions for evaluating the coupling between loop antennas have not been previously available. This paper presents straightforward analytical expressions for efficient calculation of the coupling between two circular loops at arbitrary locations. The theory is extended to the optical regime by taking into account the dispersion and loss of the material comprising the loop antenna. These analytical expressions provide insight into the physics underlying the mutual coupling phenomenon. Along with the approximate analytical expressions, a useful pseudo-analytical representation is developed which is more exact, especially in the near-field regime, and can be easily and efficiently evaluated in MATLAB via numerical integration. It is shown that full-wave simulations for a two-element array of nanoloops can take up to six hours, while the corresponding analytical and pseudo-analytical implementations derived here take less than a minute.**

***Index Terms*— Antenna theory, loop antennas, mutual coupling, nanotechnology, submillimeter wave technology.**

I. Introduction

CIRCULAR loops, along with dipoles and slots, are among the most fundamental and rigorously studied antenna geometries in the radio frequency (RF) regime. Loop antennas are inexpensive and simple to construct, and have found a wide range of practical applications including use as probes and radio receivers [1]. Coupling between loops is of interest in areas such as mine communications [2] and geological characterization [3]. In addition, coupling plays a crucial role in the design of arrays of circular loops, such as the highly directive Yagi–Uda antenna [4]. Due to advancements in manufacturing and the emerging importance of wireless communications, nanotechnology-enabled devices which operate in the terahertz, infrared, and optical regimes have received considerable attention recently. In particular, nanoantennas are extremely promising for a variety of applications including biological sensing, optical communications, and solar energy harvesting [5]. Most of the theoretical development work on optical nanoantennas has its roots in RF and microwave antennas [6], which have been studied extensively [7]. Popular antenna designs in the nanoscale include the monopole [8], dipole [9], and bow-tie [10]. Similar to the RF world, arrays of nanoantennas (mostly dipoles) have been studied for their high directivity and ability to steer light [11], [12]. Despite its fundamental importance in RF systems, the loop antenna has not received as much attention in the optical regime. In fact, exact analytical representations of the input impedance, radiation resistance, and radiation efficiency of a nanoloop antenna were not developed until 2013 [13]. While nanoloop arrays have been considered for their potential use in solar cells [14], [15] and as directive scatterers [16], a rigorous analysis of the coupling between the elements of these arrays has yet to be successfully carried out. A full-wave simulation is typically employed when designing such structures, but this approach requires a large amount of computational resources. An exact analytical representation of the coupling phenomenon would lead to a better understanding of the underlying physics and allow for extremely efficient design iterations and parametric studies.

Assuming the current distribution of a thin-wire PEC circular loop followed a Fourier cosine series enabled calculation of the input impedance and resonance properties [17]–[19]. Moreover, by finding an analytical representation of the vector potential integrals, exact near-zone and far-zone representations of the electric and magnetic field were derived [20], [21]. These equations can be applied to the nanoloops in the optical regime by extending the formulation to include the effects of dispersion and loss of the material comprising the loop. Utilizing this approach, analytical expressions for the

Manuscript received November 10, 2016; revised August 31, 2017; accepted September 8, 2017. Date of publication September 19, 2017; date of current version November 30, 2017. This work was supported in part by the Spanish Ministry of Education-Commission Fulbright Program "Salvador de Madariaga" for sponsoring the joint research collaboration under Grant PRX14/00320, in part by the Spanish and Andalusian research programs Grant TEC2013-48414-C3-01 and Grant P12-TIC-1442, in part by the Center for Nanoscale Science, and in part by an NSF Materials Research Science and Engineering Center under Grant DMR-1420620. *(Corresponding author: Jogender Nagar.)*

J. Nagar, B. Q. Lu, and D. H. Werner are with the Electrical Engineering Department, Pennsylvania State University, University Park, PA 16802 USA (e-mail: jun16e3@psu.edu; byl5088@psu.edu; dhw@psu.edu).

M. F. Pantoja is with the Electrical Engineering Department, University of Granada, 18071 Granada, Spain (e-mail: mario@ugr.es).

Color versions of one or more of the figures in this paper are available online at http://ieeexplore.ieee.org.

Digital Object Identifier 10.1109/TAP.2017.2754411

radiation properties of nanoloops were recently found in [22]. Through application of the induced electromotive force (EMF) method [7], the mutual coupling between antenna elements can be evaluated. This approach has been used to compute the coupling between dipoles [23] and slots [24]. However, due to the complexity of the integrals involved in computing coupling between loop antennas [25], [26], no fully analytical solution has previously been found for arbitrarily large loops. Wait derived expressions for the mutual coupling between electrically small loops located at the same height above a homogeneous ground when the separation distance is small by employing a quasi-static approximation [27]. The same author later extended this formulation to compute an approximate solution for two small loops separated by an arbitrary distance on the surface of an inhomogeneous ground [28]. Integral equation-based solutions were reported for the coupling between two identical coaxial loops [25] and an array of coaxial loops with different radii [26]. This was further extended to an array of loops of arbitrary radii, orientation, and location [29]. Our contribution in this paper is the development of exact analytical solutions for the mutual coupling between PEC or dispersive and lossy loops of arbitrary radii and the location which does not involve complex matrix inversions. In this paper, efficient fully analytical expressions for the mutual coupling between nanoloops are derived under the assumption that the loops are relatively far apart. In addition, an alternate and general pseudo-analytical formulation which is more accurate for closely spaced loops will be developed by utilizing the full near-zone electric fields in conjunction with the analytical current distribution of [21]. This expression can be calculated efficiently using a numerical integration routine. Timing comparisons were performed on a Dual Intel Xeon 2.3 GHz Processor with 10 cores. A full-wave solver such as the integral equation-based method implemented in FEKO [30] utilizing all 10 cores can take up to six hours to simulate while the two approaches derived in this paper take less than a minute when implemented in MATLAB and utilizing only a single core.

Section II presents a pseudo-analytical exact representation of the mutual admittances for circular nanoloops when the near-zone radiated fields are considered. Then, by employing a series of far-zone approximations, useful fully analytical expressions are developed. When the loops are in the stacked configuration, it is shown that a particularly simple expression can be derived for this important special case. Section III compares these results with those from full-wave solvers and experimental measurements and analyzes the regimes in which the assumptions are valid.

II. Theoretical Formulation

Fig. 1 shows the geometry of a circular loop with wire radius a and loop radius b, where the thin-wire approximation ($a^2 \ll b^2$, $a \ll \lambda$) is assumed. Note that for non-PEC loops the effective wavelength must be used in the thin-wire limit [32]. Under this assumption, the current is constant through the wire cross section for both PEC and non-PEC cases. The input impedance of the antenna can be derived by assuming a Fourier series representation for the current on the loop

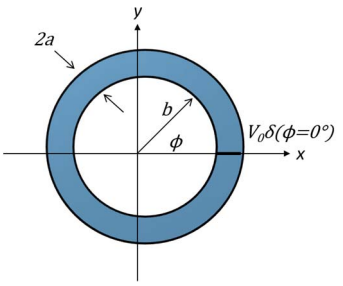

Fig. 1. Geometry of the circular loop with wire radius a and loop radius b where $a^2 \ll b^2$. For computational purposes, a delta-function voltage source with constant voltage V_0 is placed at $\phi = 0$.

when excited with a voltage source of magnitude V_0 located at $\phi = 0$ [17]

$$I(\phi) = \sum_{m=-\infty}^{\infty} I_m e^{jm\phi} = V_0 \left[\sum_{m=0}^{\infty} Y'_m \cos(m\phi) \right] \tag{1}$$

where the input admittance Y'_m for each mode is given by

$$\begin{aligned} Y'_0 &= [j\pi\eta_0 a_0 + (b/a)Z_s]^{-1} \\ Y'_m &= [j\pi\eta_0 (a_m/2) + (b/a)(Z_s/2)]^{-1} \end{aligned} \tag{2}$$

and Z_s is the characteristic impedance of the wire. Explicit representations of the a_m coefficients can be found in [17]. The computational implementation of (2) requires the solution of integrals involving Lommel-Weber and Bessel functions. An extended discussion of efficient series representations of these integrals is provided in [22]. For a PEC, the corresponding characteristic impedance of the wire is $Z_s = 0$. However, when real materials are employed in the optical regime, this characteristic impedance of the wire can be approximated by [14]

$$Z_s = \frac{\gamma}{\sigma} \frac{J_0(\gamma a)}{J_1(\gamma a)} \tag{3}$$

where J_m is a Bessel function of the first kind of order m, and the transverse propagation constant γ and conductivity σ are functions of the refractive index of the material η. The refractive index can be represented by a Drude model extended to include critical points of the band transitions as Lorentzian resonances [31], [32]. The modal coefficients for the current can be computed explicitly by

$$I_m = Y'_m V_0 = \left(Z'_m\right)^{-1} V_0. \tag{4}$$

The geometry considered for computing the radiated fields is shown in Fig. 2. The near-zone electric fields at the point (r, θ, ϕ) can be determined based on the source points $(b, \frac{\pi}{2}, \phi')$. The distance from a source point on the loop to an arbitrary field point is given by

$$\begin{aligned} R' &= \sqrt{R^2 - 2b\sin\theta\cos(\phi - \phi')} \\ R &= \sqrt{r^2 + b^2}. \end{aligned} \tag{5}$$

The integrations involved in the vector potentials can be evaluated analytically, as demonstrated in [20]. Using these vector potentials, the electric field components at a point

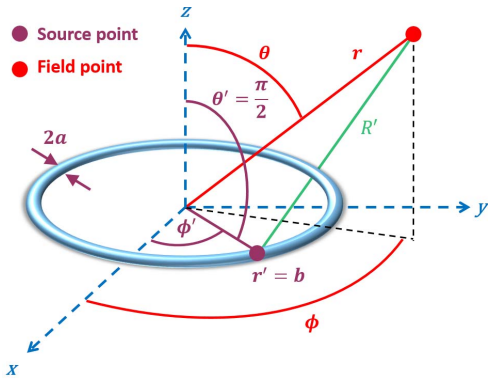

Fig. 2. Geometry of the thin circular loop antenna. The near-zone radiated fields can be evaluated at the point (r, θ, ϕ).

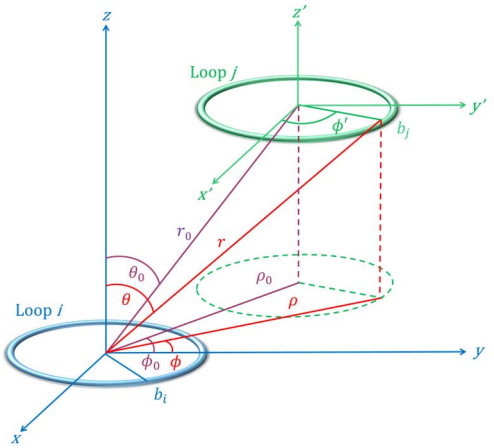

Fig. 3. Geometry of the active loop i and passive loop j. Loop j is centered at (x_0, y_0, z_0). The loop represented by a dashed line is the projection of the passive loop j onto the xy-plane. The vector $(\hat{r}, \hat{\theta}, \hat{\phi})$ points from the center of loop i to a point on the circumference of loop j while $(\hat{r}_0, \hat{\theta}_0, \hat{\phi}_0)$ points from center to center.

(r, θ, ϕ) are given in (6), as shown at the bottom of this page, where $h_m^{(2)}(k_0 R)$ are spherical Hankel functions of the second kind. By employing the appropriate asymptotic expansions, the electric fields in the far-zone may be expressed in spherical coordinates (θ, ϕ) as [20]

$$
\begin{aligned}
E_r &\approx 0 \\
E_\theta &\approx -\frac{\eta_0 e^{-jk_0 r}\cot\theta}{2r}\sum_{m=1}^{\infty} m j^m I_m \sin(m\phi) J_m(k_b \sin\theta) \\
E_\phi &\approx -\frac{\eta_0 e^{-jk_0 r} k_b}{2r}\sum_{m=0}^{\infty} j^m I_m \cos(m\phi) J_m'(k_b \sin\theta) \qquad (7)
\end{aligned}
$$

where J_m' is the derivative of the Bessel function of the first kind with respect to the argument. In this paper, the induced current on a passive loop due to radiation from an active loop will be calculated under a variety of geometrical configurations and approximations. First, the full near-zone fields of (6) will be utilized to construct a pseudo-analytical representation for the induced current when the two loops are at arbitrary locations. Then, using a series of far-field approximations and the far-zone fields of (7), it will be shown that an exact analytical representation can be derived. Finally, an analytical expression for the induced current for the special case of a stacked loop configuration will be presented.

A. Pseudo-Analytical Representation of Induced Current

The geometry to be considered when computing the mutual coupling is shown in Fig. 3. The unprimed coordinate system (x, y, z) is defined with origin at the center of loop i while the primed coordinate system (x', y', z') is defined with origin at the center of loop j. The dimensions for each individual loop are indicated in Fig. 1, where for loop i the radius of the wire and loop is a_i and b_i respectively. The vector denoted by $(\hat{r}, \hat{\theta}, \hat{\phi})$ is directed from the center of loop i to a point on loop j while $(\hat{r}_0, \hat{\theta}_0, \hat{\phi}_0)$ points from center to center.

$$
\begin{aligned}
E_r(r,\theta,\phi) &= \frac{\eta_0 k_0^2 b \sin\theta}{4}\left\{\sum_{m=1}^{\infty}\sum_{\substack{n=1\\ m-n=2k\\ k=0,1,\ldots}}^{m}\left(\frac{k_0^2 br\sin\theta}{2}\right)^{m-1}\sin(n\phi)\left[(k_0 b)^2 C_{\mathrm{mn}}^3\frac{h_{m+1}^{(2)}(k_0R)}{(k_0R)^{m+1}} - C_{\mathrm{mn}}^4\frac{h_m^{(2)}(k_0R)}{(k_0R)^m}\right]\right\} \\
E_\theta(r,\theta,\phi) &= \frac{\eta_0 k_0^2 b \cos\theta}{4}\left\{\sum_{m=1}^{\infty}\sum_{\substack{n=1\\ m-n=2k\\ k=0,1,\ldots}}^{m}\left(\frac{k_0^2 br\sin\theta}{2}\right)^{m-1}\sin(n\phi)\left[C_{\mathrm{mn}}^5\frac{h_m^{(2)}(k_0R)}{(k_0R)^m} - C_{\mathrm{mn}}^3\frac{h_{m-1}^{(2)}(k_0R)}{(k_0R)^{m-1}}\right]\right\} \\
E_\phi(r,\theta,\phi) &= \frac{\eta_0 k_0^2 b}{4}\left\{\sum_{m=1}^{\infty}\sum_{\substack{n=0\\ m-n=2k\\ k=0,1,\ldots}}^{m}\left(\frac{k_0^2 br\sin\theta}{2}\right)^{m-1}\cos(n\phi)\left[C_{\mathrm{mn}}^6\frac{h_m^{(2)}(k_0R)}{(k_0R)^m} - C_{\mathrm{mn}}^2\frac{h_{m-1}^{(2)}(k_0R)}{(k_0R)^{m-1}}\right]\right\} \\
C_{\mathrm{mn}}^2 &= I_n\frac{m}{[(m-n)/2]![(m+n)/2]!}; \quad C_{\mathrm{mn}}^3 = I_n\frac{n}{[(m-n)/2]![(m+n)/2]!} \\
C_{\mathrm{mn}}^4 &= (m+1)C_{\mathrm{mn}}^3; \quad C_{\mathrm{mn}}^5 = mC_{\mathrm{mn}}^3; \quad C_{\mathrm{mn}}^6 = nC_{\mathrm{mn}}^3 \qquad (6)
\end{aligned}
$$

The vector defined by $(\hat{\rho}, \pi/2, \hat{\phi})$ is directed from the center of loop i to a point on loop j projected onto the xy-plane, as depicted by the dashed lines in Fig. 3. Similarly, the vector $(\hat{\rho}_0, \pi/2, \hat{\phi}_0)$ points from the center of loop i to the center of the projected loop j. The induced EMF method can be used to compute the induced current at the angle Φ' on the passive loop with index j due to an active loop with index i, as represented by the following:

$$I_j(\Phi') = V_{ij}\left[\sum_{p=0}^{\infty} Y'_{p,j}\cos(p(\Phi'-\phi'))\right] \tag{8}$$

where $Y'_{p,j}$ is the pth modal admittance for loop j and, for convenience, we have explicitly separated the term proportional to the induced voltage V_{ij} as

$$V_{ij} \equiv b_j \int_0^{2\pi} \vec{E}_i \cdot \hat{t}\, d\phi'. \tag{9}$$

The tangential vector in the coordinate system of loop j is

$$\hat{t} = -\sin\phi'\hat{x} + \cos\phi'\hat{y}. \tag{10}$$

Moreover, the dot products between the spherical coordinates and the tangent vector are given by

$$\begin{aligned}
\hat{r}\cdot\hat{t} &= \frac{1}{r}(-x\sin\phi' + y\cos\phi')\\
\hat{\theta}\cdot\hat{t} &= \frac{z}{r\rho}(-x\sin\phi' + y\cos\phi')\\
\hat{\phi}\cdot\hat{t} &= \frac{1}{\rho}(y\sin\phi' + x\cos\phi')
\end{aligned} \tag{11}$$

where $x = x_0 + b_j\cos\phi'$, $y = y_0 + b_j\sin\phi'$, $r = \sqrt{x^2+y^2+z_0^2}$ and $\rho = \sqrt{x^2+y^2}$. A pseudo-analytical representation for the induced current, which includes the exact near-zone electric fields, may be obtained by combining (6) with (8)–(11). The resulting expression is given in (12), as shown at the bottom of this page, where $\theta = \cos^{-1}\frac{z_0}{r}$ and $\phi = \tan^{-1}\frac{y}{x}$ and where it is noted that numerical integration is required to evaluate the terms $F_{\mathrm{mnp}}(\Phi')$. The summation over m and n in the integrand of this expression corresponds to the induced voltage at the terminals of antenna j due to radiation from antenna i. The modified notation $C_{\mathrm{mn},i}$ is used to refer to the C_{mn} coefficients for antenna i. In contrast, the summation over p involves the modal admittances for antenna j given by $Y'_{p,j}$. The self-admittance of loop i is given by

$$Y_{ii} = \sum_{p=0}^{\infty} Y'_{p,i}. \tag{13}$$

The mutual admittance Y_{ji} can be found by applying a voltage source V_i to loop i placed at $\Phi = 0$ and shorting loop j

$$Y_{ji} = \frac{I_j(\Phi'=0)}{V_i}. \tag{14}$$

Finally, for an array of N loops, the current at the input terminals of loop j is given by

$$I_j = \sum_{j=1}^{N} Y_{ji}V_i. \tag{15}$$

B. Analytical Representation of Induced Current

Using a numerical suite such as MATLAB, the modal admittances of (2) can be easily determined. Then the induced current can be computed by performing the numerical integration required to evaluate (12). However, one of the drawbacks associated with this pseudo-analytical representation is that it does not provide any physical insight into the behavior of the problem. Furthermore, to compute the numerical integral accurately a sophisticated routine such as global adaptive quadrature is required [33]. Therefore, an analytical representation is desired. When using the near-zone fields, the resulting integral in (12) is extremely complex and an analytic representation for the general form has not been found. Therefore, the far-zone field expressions of (7) will be employed along with a number of asymptotic approximations. It will be shown that these assumptions hold remarkably well even when the loops are relatively closely spaced. Substituting the far-zone

$$I_j(\Phi') = \frac{\eta_0 k_0^2 b_i b_j}{4}\sum_{p=0}^{\infty} Y'_{p,j}\sum_{m=1}^{\infty}\sum_{\substack{n=1\\ m-n=2k\\ k=0,1,\ldots}}^{m}\left(\frac{k_0^2 b_i}{2}\right)^{m-1} F_{\mathrm{mnp}}(\Phi')$$

$$\begin{aligned}
F_{\mathrm{mnp}}(\Phi') = \int_0^{2\pi} &\cos(p(\Phi'-\phi'))(r\sin\theta)^{m-1}\\
&\times\left[\frac{1}{r}\sin(\theta)\sin(n\phi)(-x\sin\phi' + y\cos\phi')\left(k_0^2 b_i^2 C^3_{\mathrm{mn},i}\frac{h^{(2)}_{m+1}(k_0R)}{(k_0R)^{m+1}} - C^4_{\mathrm{mn},i}\frac{h^{(2)}_m(k_0R)}{(k_0R)^m}\right)\right.\\
&+\frac{z}{r\rho}\cos(\theta)\sin(n\phi)(-x\sin\phi' + y\cos\phi')\left(C^5_{\mathrm{mn},i}\frac{h^{(2)}_m(k_0R)}{(k_0R)^m} - C^3_{\mathrm{mn},i}\frac{h^{(2)}_{m-1}(k_0R)}{(k_0R)^{m-1}}\right)\\
&\left.+\frac{1}{\rho}\cos(\theta)\cos(n\phi)(y\sin\phi' + x\cos\phi')\left(C^6_{\mathrm{mn},i}\frac{h^{(2)}_m(k_0R)}{(k_0R)^m} - C^2_{\mathrm{mn},i}\frac{h^{(2)}_{m-1}(k_0R)}{(k_0R)^{m-1}}\right)\right]d\phi'
\end{aligned} \tag{12}$$

representations for the electric fields into (8)–(11) leads to an expression for the θ-component of the induced current, which is given by the following:

$$I_{\theta,j}(\Phi') = -\frac{\eta_0 z_0^2 b_j \rho_0}{2} \sum_{p=0}^{\infty} Y'_p \sum_{n=1}^{\infty} n j^n I_{n,i} F_{\mathrm{np}}(\Phi')$$

$$F_{\mathrm{np}}(\Phi') = \int_0^{2\pi} \frac{e^{-jk_0 r}}{r^2 \rho^2} \sin(\phi_0 - \phi') \cdot \sin(n\phi) J_n\left(\frac{k_0 b_i \rho}{r}\right) \cos(p(\Phi' - \phi'))d\phi'. \quad (16)$$

In (16), the two parameters r and ρ depend on the variable of integration ϕ'. At this point in the analysis several assumptions will be made which reduce the complexity of the integral in (16) such that it becomes tractable. If the two loops are sufficiently far apart, the following far-zone approximations hold:

$$\rho \approx \begin{cases} \rho_0 & \text{for amplitude terms} \\ \rho_0\left(1 + \dfrac{b_j}{\rho_0}\cos(\phi_0 - \phi')\right) & \text{for phase terms} \end{cases} \quad (17)$$

$$r \approx \begin{cases} r_0 = \sqrt{\rho_0^2 + z_0^2} & \text{for amplitude terms} \\ \sqrt{\rho_0^2 + z_0^2}\left(1 + \dfrac{b_j \rho_0}{r_0^2}\cos(\phi_0 - \phi')\right) & \text{for phase terms.} \end{cases} \quad (18)$$

Another major complication with the integration of (16) lies in the fact that ϕ depends on ϕ'. When the two loops are not stacked or nearly on top of each other, the approximation $\phi = \phi_0$ can also be employed. The stacked loop case will be discussed separately in the following section. Using these approximations, the θ-component of the induced current can be reduced to the form

$$I_{\theta,j}(\Phi') = -\frac{\eta_0 b_j z_0^2}{2\rho_0 r_0^2} e^{-jk_0 r_0} \sum_{p=0}^{\infty} Y'_{p,j} \cdot \sum_{n=1}^{\infty} n j^n I_{n,i} J_n\left(\frac{k_0 b_i \rho_0}{r_0}\right) \sin(n\phi_0) FS_p(\Phi')$$

$$FS_p(\Phi') = \int_0^{2\pi} e^{-j\frac{k_0 b_j \rho_0}{r_0}\cos(\phi_0 - \phi')} \cdot \sin(\phi_0 - \phi')\sin(p(\Phi' - \phi'))d\phi'. \quad (19)$$

Now the integrand of $FS_p(\Phi')$is explicitly in terms of ϕ'. By representing the sine and cosine functions as complex exponentials and using the Bessel generating function [34], this integral can be evaluated analytically. The ϕ-component of the induced current can be derived by using the same approximations. The final expression for the total induced current due to E_θ and E_ϕ is given by (20), as shown at the bottom of this page.

It will be shown in Section III that the radial component of the electric field has a surprisingly large contribution to the induced current, even when the loop is relatively far away. By employing a series of approximations in which we assume that the passive loop is sufficiently far away from the active loop, the contribution of the radial electric field component can be evaluated analytically. To this end, the following approximations were made:

$$R \approx r \approx \begin{cases} r_0 & \text{for amplitude terms} \\ r_0\left(1 + \dfrac{b_j \rho_0}{r_0^2}\cos(\phi_0 - \phi')\right) & \text{for phase terms} \end{cases}$$
$$\theta \approx \theta_0$$
$$\phi \approx \phi_0 \quad (21)$$

In addition, the large argument asymptotic limit of the spherical Hankel function of the second kind is employed

$$\lim_{x\to\infty} h_m^{(2)}(x) = j^{m+1}\frac{e^{-jx}}{x}. \quad (22)$$

This approximation is valid when the loops are adequately separated since the argument under consideration is $k_0 R$, which in the RF or optical regime would be extremely large. The resulting expression for the radial contribution is given by

$$I_{r,j}(\Phi') = \frac{\eta_0 b_i b_j \rho_0^2}{4 r_0^4} \sum_{p=0}^{\infty} Y'_{p,j} \sum_{m=1}^{\infty} \sum_{\substack{n=1 \\ m-n=2k \\ k=0,1,2\ldots}}^{m} \sin(n\phi_0) \cdot \left[\frac{k_0 b_i \sin\theta_0}{2}\right]^{m-1} j^{m+1} e^{-jk_0 r_0} \cdot \left[\frac{jk_0 b_i^2 C^3_{\mathrm{mn},i}}{r_0} - C^4_{\mathrm{mn},i}\right] FC_p(\Phi')$$

$$FC_p(\Phi') = \int_0^{2\pi} e^{-j\frac{k_0 b_j \rho_0}{r_0}\cos(\phi_0 - \phi')} \cdot \sin(\phi_0 - \phi')\cos(p(\Phi' - \phi'))d\phi'. \quad (23)$$

The integral $FC_p(\Phi')$ that appears in (23) is similar to that given in (19) and its analytical solution can be found

$$I_j(\Phi') = -\frac{\eta_0 \pi}{r_0} e^{-jk_0 r_0} \sum_{p=0}^{\infty} Y'_{p,j}(-1)^p (j)^{p-1} \sum_{n=0}^{\infty} j^n I_{n,i} \times \left[\frac{z_0^2}{\rho_0^2 k_0} np \sin(n\phi_0) J_p\left(\frac{k_0 b_i \rho_0}{r_0}\right) J_n\left(\frac{k_0 b_i \rho_0}{r_0}\right) \sin(p(\Phi' - \phi_0)) + k_0 b_i b_j \left(j\frac{b_j}{\rho_0} J_p\left(\frac{k_0 b_i \rho_0}{r_0}\right) - J'_n\left(\frac{k_0 b_i \rho_0}{r_0}\right)\right) \cos(n\phi_0) J'_p\left(\frac{k_0 b_j \rho_0}{r_0}\right) \cos(p(\Phi' - \phi_0))\right] \quad (20)$$

through analogous mathematical manipulations, as outlined in Appendix A.

The final induced current due to the contribution of all three spherical components is given in (24), as shown at the bottom of this page, where we define $D_i = (k_0 b_i \rho_0 / r_0)$ and $D_j = (k_0 b_j \rho_0 / r_0)$. Moreover, for the special case when the loops are coplanar, the expression reduces to (25), as shown at the bottom of this page. Full details of the derivation will be presented in Appendix A. While these expressions appear daunting, the computation of the Bessel functions in a numerical suite such as MATLAB is extremely efficient [35]. Note that this expression is a summation of sinusoids and cosinusoids, similar to the decomposition originally assumed in (1). Therefore, the resulting far-field can be computed using the expressions in (7) and array factor theory [7]. In general, for N loops with the ith loop located at $(x_{0,i}, y_{0,i}, z_{0,i})$, the total electric field can be computed as (25)

$$E(\theta,\phi) = \sum_{i=1}^{N} E_i(\theta,\phi) e^{jk_0[x_{0,i}\sin\theta\cos\phi + y_{0,i}\sin\theta\sin\phi + x_{0,i}\cos\theta]} \tag{26}$$

where $E_i(\theta,\phi)$ is the radiated electric field from the ith loop given explicitly in (7).

C. Analytical Representation of Induced Current in Stacked Loop Case

Now consider the special case of multiple loops stacked on top of each other, a popular configuration found in Yagi–Uda arrays [11]. As shown in Fig. 4, the critical observation is that the angle ϕ in unprimed coordinates is exactly the same as the variable of integration ϕ' in primed coordinates. In this case only the E_ϕ component contributes since the dot products $\hat{\theta}\cdot\hat{t}$ and $\hat{r}\cdot\hat{t}$ are both equal to zero. After a series of mathematical manipulations, it can be shown that the induced current in this case can be expressed in a particularly simple form

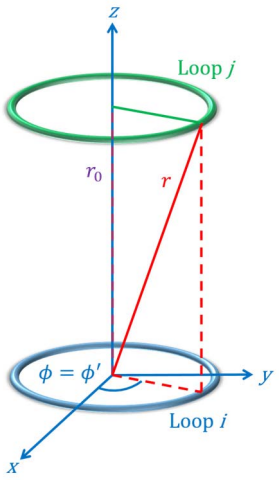

Fig. 4. Geometry of a passive loop j placed directly above the active loop i.

$$I_j(\Phi') = -\frac{\eta_0 k_0 b_i b_j \pi}{2r} e^{-jk_0 r} \cdot \left[\sum_{p=0}^{\infty} j^p I_{p,i} J'_p\left(\frac{k_0 b_i b_j}{r}\right) Y'_{p,j}(\cos(p\Phi')) + I_{0,i} Y'_{0,j} J'_0\left(\frac{k_0 b_i b_j}{r}\right) \right] \tag{27}$$

where $r = (r_0^2 + b_j^2)^{1/2}$ which is independent of ϕ' in the stacked case. Details of this derivation are provided in Appendix B.

$$I_j(\Phi') = -\frac{\eta_0\pi}{r_0} e^{-jk_0 r_0} \sum_{p=0}^{\infty} Y'_{p,j}(-1)^p (j)^{p-1} \times \left\{ \begin{array}{l} \displaystyle\sum_{n=0}^{\infty} \left[j^n I_{n,i} \frac{z_0^2}{\rho_0^2 k_0} np \sin(n\phi_0) J_p(D_j) J_n(D_i) \sin(p(\Phi'-\phi_0)) + k_0 b_i b_j \left[j\frac{b_j}{\rho_0} J_p(D_j) - J'_p(D_j) \right] \right. \\ \qquad \left. \times J'_n(D_i)\cos(n\phi_0)\cos(p(\Phi'-\phi_0)) \right] \\ \displaystyle -\frac{\rho_0 b_i}{2r_0^2 k_0} \sum_{m=1}^{\infty} \sum_{\substack{n=1 \\ m-n=2k \\ k=0,1,2\ldots}}^{m} j^{m+1} \sin(n\phi_0) \left[\frac{k_0 b_i \sin\theta_0}{2}\right]^{m-1} \left[\frac{jk_0 b_i^2 C^3_{\mathrm{mn},i}}{r_0} - C^4_{\mathrm{mn},i} \right] p J_p(D_j) \sin(p(\Phi'-\phi_0)) \end{array} \right\} \tag{24}$$

$$I_j(\Phi') = -\frac{\eta_0\pi}{2r_0 k_0} e^{-jk_0 r_0} \sum_{p=0}^{\infty} Y'_{p,j}(-1)^p j^{p-1} \times \left\{ \begin{array}{l} \displaystyle 2k_0^2 b_j b_i \cos(p(\Phi'-\phi_0)) \sum_{n=0}^{\infty} \left[I_{n,i}\cos(n\phi_0) j^n \left[j\frac{b_j}{r_0} J_p(k_0 b_j) - J'_p(k_0 b_j) \right] J'_n(k_0 b_i) \right] \\ \displaystyle -\frac{b_i}{r_0}\sin(p(\Phi'-\phi_0)) \sum_{m=1}^{\infty} \sum_{\substack{n=1 \\ m-n=2k \\ k=0,1,2\ldots}}^{m} \left\{ j^{m+1}\sin(n\phi_0) \left[\frac{k_0 b_i}{2}\right]^{m-1} \left[\frac{jk_0 b_i^2 C^3_{\mathrm{mn},i}}{r_0} - C^4_{\mathrm{mn},i} \right] p J_p(k_0 b_j) \right\} \end{array} \right\} \tag{25}$$

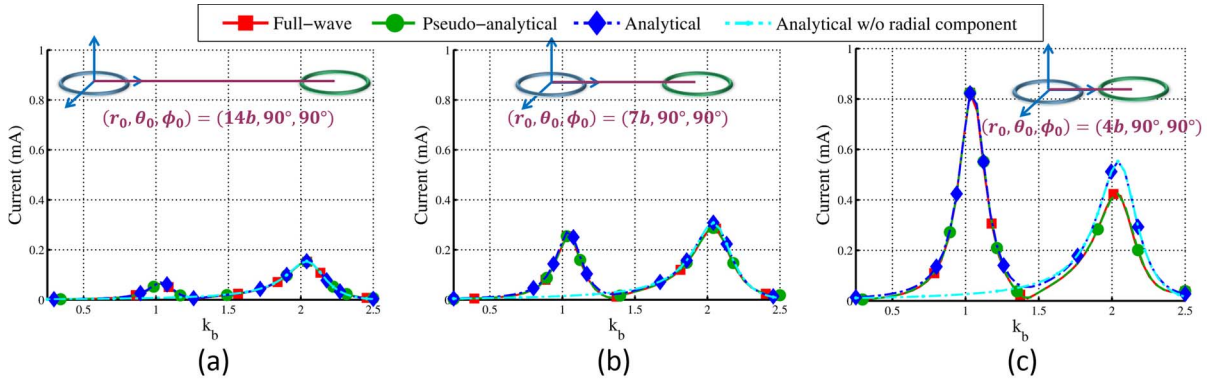

Fig. 5. Comparison between FEKO, pseudo-analytical expression with numerical integration performed in MATLAB, and the fully analytical expressions evaluated in MATLAB with and without the radial contribution for two PEC loops ($\Omega = 12$) separated at an angle $(\theta_0, \phi_0) = (90°, 90°)$ and a distance of (a) $14b$, (b) $7b$, and (c) $4b$. The agreement between the analytical solution and the results produced by the other two methods is much better when including the radial contribution, but the analytical expressions start to break down as the loops get closer to each other.

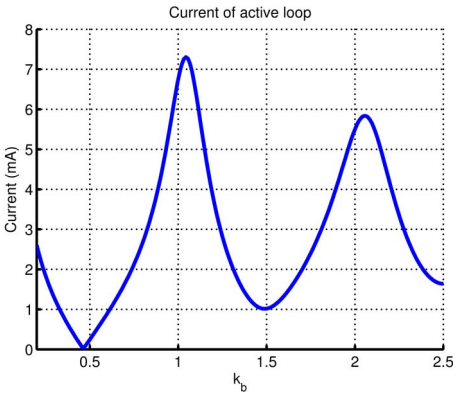

Fig. 6. Current distribution on an active PEC loop at the feed point. This is equivalent to the input admittance when a feed voltage of V_0 is assumed. Peaks can be observed slightly above $k_b = 1$ and $k_b = 2$.

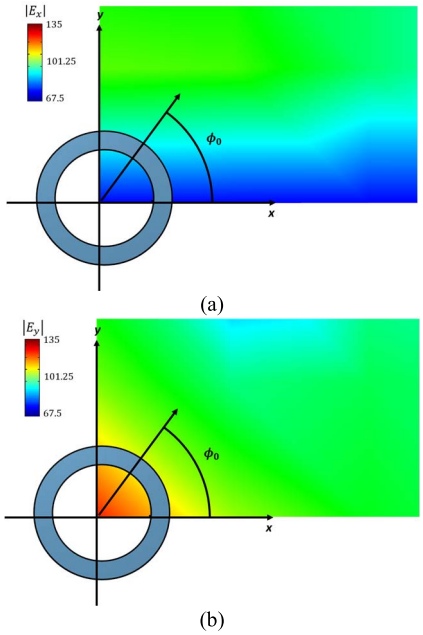

Fig. 7. Near-fields in the xy-plane for a PEC loop ($\Omega = 12$, $k_b = 1$) where (a) shows E_x and (b) shows E_y. As can be seen, the radial component in the $\phi_0 = 0°$ direction E_x rapidly falls off with distance while the radial component in the $\phi_0 = 90°$ direction E_x falls off much more gradually.

III. Results

The validation of the analytical expressions derived in the previous section will be carried out by considering the coupling between two PEC loops with $\Phi' = 0$ under a variety of geometrical configurations. The loop ($b_1 = b_2 = b$) and wire radii ($a_1 = a_2 = a$) will be chosen such that the thickness measure [19] $\Omega = 2 \ln (2\pi b/a)$ is equal to 12. The results will be plotted in terms of $k_b = 2\pi b/\lambda$, such that the resulting curves universally apply to PEC loops of any radius b. To test the validity of these expressions in the optical regime, gold nanoloops with circumferences of 600 and 3000 nm will be considered. The gold material is modeled according to [22]. It has been found from numerical experimentation that the analytical expressions match FEKO well when $r_0 > 4b$ for the PEC case. For gold, there is good agreement when $r_0 > 10b$ for a 600 nm circumference nanoloop and when $r_0 > 7b$ for a 3000 nm circumference nanoloop. When $\theta_0 < 10°$ the stacked loop approximation $\phi = \phi'$ holds fairly well; otherwise, the more general approximation $\phi = \phi_0$ should be used. Note that these rules of thumb were derived over the range $k_b \in [0.01, 2.5]$ for the 3000 nm circumference gold loop and $k_b \in [0.01, 0.5]$ for the 600 nm circumference gold loop. Above these frequencies the extinction coefficient of gold is greater than eight and the loops are extremely lossy [22], resulting in very little coupling between elements. For the PEC case, very good agreement was observed over the range $k_b \in [0.01, 5.0]$, above which the thin-wire assumption no longer holds.

The analytical expressions given in (24), (25), and (27) were implemented in MATLAB and the comparisons were made with the exact numerical integration of (12) and the full-wave integral equation solver FEKO [27]. The tests were run on a Dual Intel Xeon Processor with 10 cores. FEKO was run in parallel mode utilizing all 10 cores, while the other simulation methods used only a single core. Table I provides a summary of the computational resources required for each method. As can be seen, the full-wave simulation method took almost

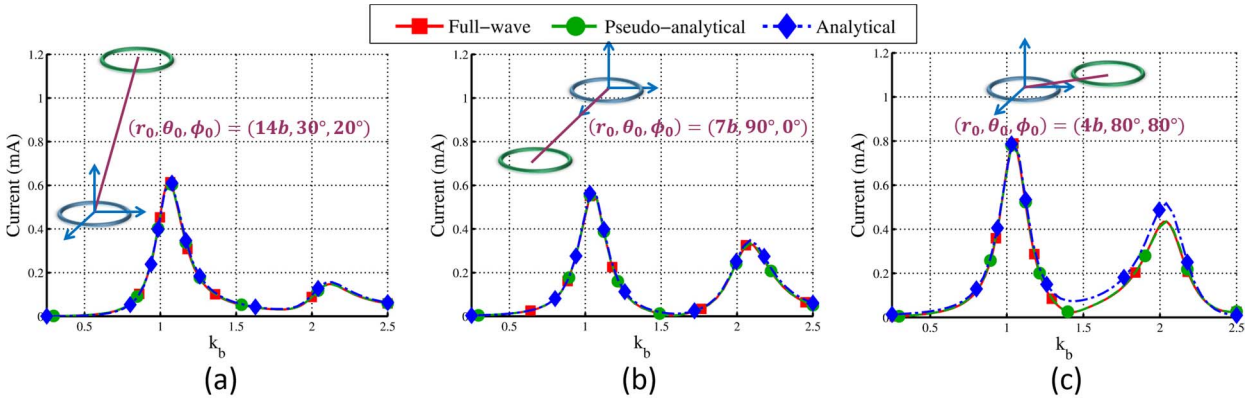

Fig. 8. Comparison between FEKO, pseudo-analytical expression with numerical integration performed in MATLAB, and the fully analytical expressions evaluated in MATLAB for (a) $(r_0, \theta_0, \phi_0) = (14b, 30°, 20°)$, (b) $(r_0, \theta_0, \phi_0) = (7b, 90°, 0°)$, and (c) $(r_0, \theta_0, \phi_0) = (4b, 80°, 80°)$. There is extremely good agreement between the different methods until r_0 approaches $4b$.

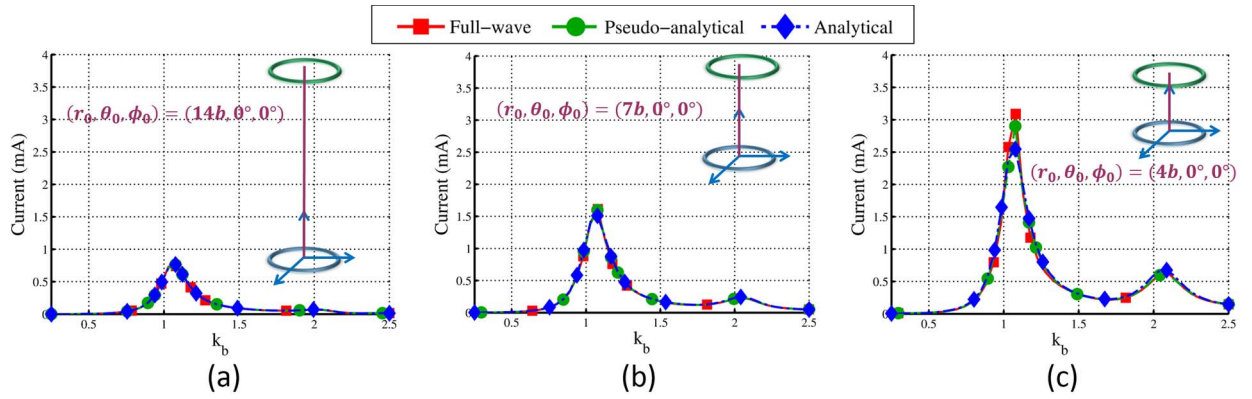

Fig. 9. Comparison between FEKO, pseudo-analytical expression with numerical integration performed in MATLAB, and the fully analytical expressions evaluated in MATLAB for the stacked configuration with (a) $r_0 = 14b$, (b) $r_0 = 7b$, and (c) $r_0 = 4b$. The magnitude of the first peak for the analytical solution is not as accurate for $r_0 = 4b$.

TABLE I
COMPARISON OF REQUIRED COMPUTATIONAL RESOURCES

Method	Time	Memory
Full-wave	5.9 hours	8.2 GB
Pseudo-analytical	33 seconds	1 GB + 34 MB
Analytical (general)	11 seconds	1 GB + 20 MB
Analytical (stacked)	0.1 seconds	1 GB + 2 MB

six hours to complete. The pseudo-analytical method took 33 s, and the fully analytical solution required 11 s. For the stacked configuration, the simplified expression required only 0.1 s to evaluate. There is also a savings in peak memory usage. The full-wave solver requires 8.2 GB of memory. Running MATLAB itself requires 1 GB of memory. In addition to this, the numerical integration-based solution requires 14 MB while the analytical solutions require 7 and 2 MB for the general and stacked cases, respectively.

Fig. 5 shows a comparison between the induced current as predicted by FEKO, the pseudo-analytical expression (16) requiring numerical integration, and the analytical representation of (24) when the r-component of the radiated field is neglected for three different loop separations and $(\theta_0, \phi_0) = (90°, 90°)$. As seen in these plots, there are peaks in the induced current that occur slightly above $k_b = 1$ and $k_b = 2$. This can be understood by considering the active current on the loop, as presented in Fig. 6. As shown explicitly in (8), there are two major contributions to the induced current. The first is proportional to the induced voltage due to radiation from the active loop. The second is the input admittance of the passive loop, which is proportional to the current of a loop driven by a voltage source. Strong peaks can be seen in the active current of Fig. 6 slightly above $k_b = 1$ and $k_b = 2$. The effect of the induced voltage is to modulate the amplitude of those peaks. The induced voltage at $k_b = 1$ increases as the interloop separation decreases from $r_0 = 14b$ to $r_0 = 4b$, which explains the relative levels of the maxima seen in Fig. 5. As can be seen, the pseudo-analytical method with numerical integration and the results from FEKO match almost exactly, which is to be expected since the exact expressions are employed and no far-field assumptions have been made. However, the fully analytical expressions (without considering the radial component) do not predict the existence of the first peak. Interestingly, the first maximum is caused by the radial component of the electric field, which gets larger as the distance between the loops decreases.

Through numerical experimentation, it was observed that the radial component has a significant contribution for

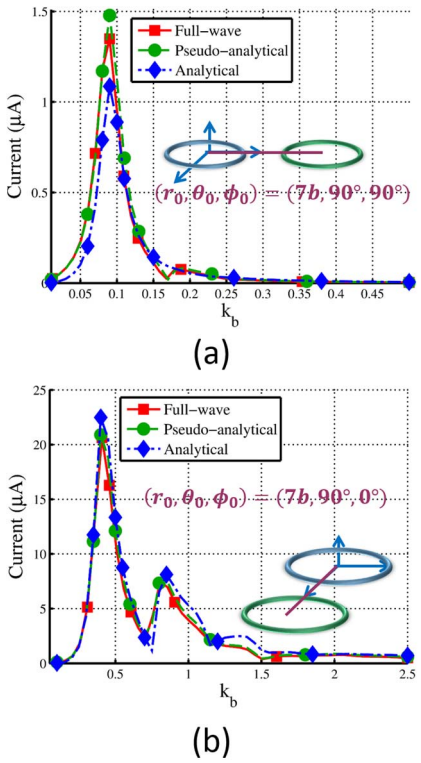

Fig. 10. Comparison between FEKO, pseudo-analytical expression with numerical integration performed in MATLAB, and the fully analytical expressions evaluated in MATLAB for (a) gold nanoloop with circumference 600 nm where $(r_0, \theta_0, \phi_0) = (7b, 90°, 90°)$ and (b) gold nanoloop with circumference 3000 nm where $(r_0, \theta_0, \phi_0) = (7b, 90°, 0°)$. For both cases the agreement between all three methods is reasonably good.

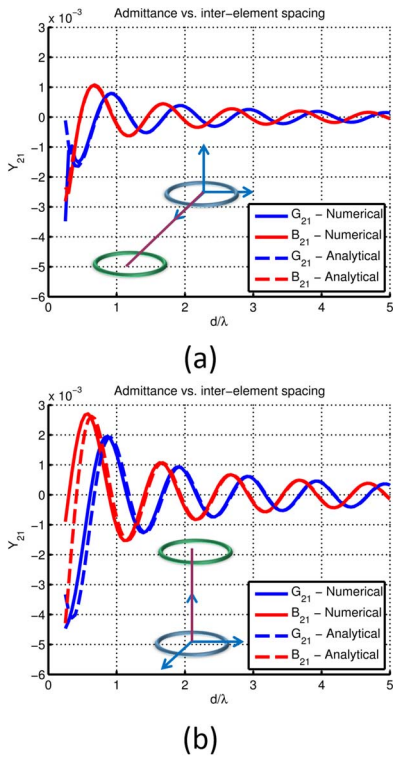

Fig. 11. Mutual admittance versus interelement spacing for PEC loops ($\Omega = 12$) where (a) $(\theta_0, \phi_0) = (90°, 0°)$ and (b) $(\theta_0, \phi_0) = (0°, 0°)$ using the numerical and fully analytical expressions.

$(\theta_0, \phi_0) = (90°, 90°)$, but is not as significant for $(\theta_0, \phi_0) = (90°, 0°)$. This can be explained by examining the radial component of the near-field of a single loop, as shown in Fig. 7. The radial component rapidly falls off in the $\phi_0 = 0°$ direction, as shown in Fig. 7(a), but falls off much more gradually in the $\phi_0 = 90°$ direction, as shown in Fig. 7(b). As indicated in Fig. 5, if the analytical expression including the radial component (24) is used, the first peak can be accurately predicted. However, the agreement starts to degrade as the loop separation decreases. To further test the generality of the analytical expressions, a series of comparisons for various cases is presented in Fig. 8, while a comparison for the special case of the stacked configuration given in (34) is shown in Fig. 9. The pseudo-analytical expression agrees very well with FEKO for all cases, while the fully analytical representation starts to deviate a bit when the interloop spacing is reduced to $4b$.

Next the analytical expressions will be tested on a gold nanoloop. For the PEC case, the maximum value of $k_b = (2\pi b/\lambda)$ considered was 2.5 and universal curves for any circumference and frequency were plotted. However, due to dispersion the antenna parameters of a gold nanoloop depend explicitly on both the loop circumference and frequency. For a gold nanoloop of circumference 600 nm, a maximum k_b of 0.5 (250 THz) will be considered. Above this frequency, the 600 nm loop has a radiation efficiency of less than 0.01% [22]. A larger gold nanoloop of circumference 3000 nm with a maximum k_b of 2.5 (250 THz) will also be considered. Fig. 10 shows good agreement between the three methods considered for the case of (a) 600 nm nanoloops with $(r_0, \theta_0, \phi_0) = (7b, 90°, 90°)$ and (b) 3000 nm nanoloops with $(r_0, \theta_0, \phi_0) = (7b, 90°, 0°)$.

Now that the analytical results have been verified, a study of the mutual admittance versus interelement spacing will be performed using both the pseudo and fully analytical representations for the induced current. The mutual conductance G_{21} and susceptance B_{21} are shown in Fig. 11 (a) and (b), respectively, as a function of interelement spacing for two PEC loops where $(\theta_0, \phi_0) = (90°, 0°)$ and $(\theta_0, \phi_0) = (0°, 0°)$. The purely analytical results agree very well with the pseudo-analytical results when the interelement spacing d exceeds about 0.5λ. Below this value, there is a slight discrepancy in the susceptance for the stacked configuration. Fig. 12 (a) and (b) show the mutual admittance versus interelement spacing for $(\theta_0, \phi_0) = (90°, 0°)$ and $(\theta_0, \phi_0) = (0°, 0°)$, this time for a gold nanoloop with a circumference of 600 nm. Again, for both cases there is good agreement for $d > 0.5\lambda$ with discrepancies in the susceptance below this distance. These discrepancies are likely due to near-field capacitive coupling which is not included in the analytical model.

In order to validate these expressions further, two copper loops designed to operate at 2 GHz and fed by coaxial cables were constructed. As shown in Fig. 13, a network analyzer was used to measure the S_{21} over a frequency range of 1.25–3 GHz as the interloop separation was varied. Two full-wave FEKO models were created: one which includes the

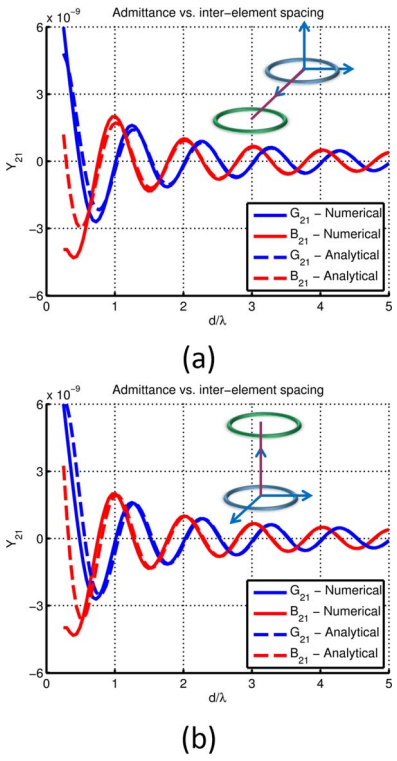

Fig. 12. Mutual admittance versus interelement spacing for gold nanoloops with circumference 600 nm ($\Omega = 12$) where (a) $(\theta_0, \phi_0) = (90°, 0°)$ and (b) $(\theta_0, \phi_0) = (0°, 0°)$ using the numerical and fully analytical expressions.

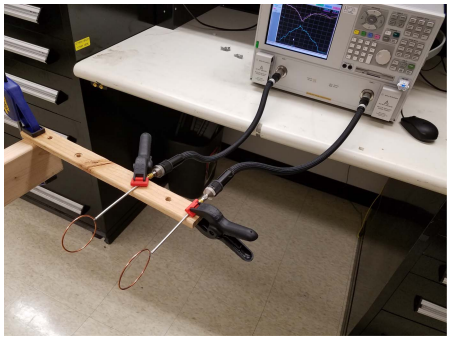

Fig. 13. Photograph of experimental setup for S_{21} measurements.

coaxial cable used in the measurements and one with an ideal voltage source. The analytical theory developed in this paper applies for an ideal voltage source and does not include any additional effects due to the presence of the coaxial cables. A comparison between the measured results, the two full-wave FEKO simulations, and the pseudo-analytical model is shown in Fig. 14 for interloop separations of (a) $2b$, (b) $6b$, and (c) $10b$. As can be seen, there is excellent agreement between the measured results and the full-wave results with a coax cable. In addition, there is excellent agreement between the full-wave and analytical results with a voltage source.

A large number of useful parameters can be calculated once the mutual admittance matrix is computed, including directivity patterns, direction-of-arrival estimation competence

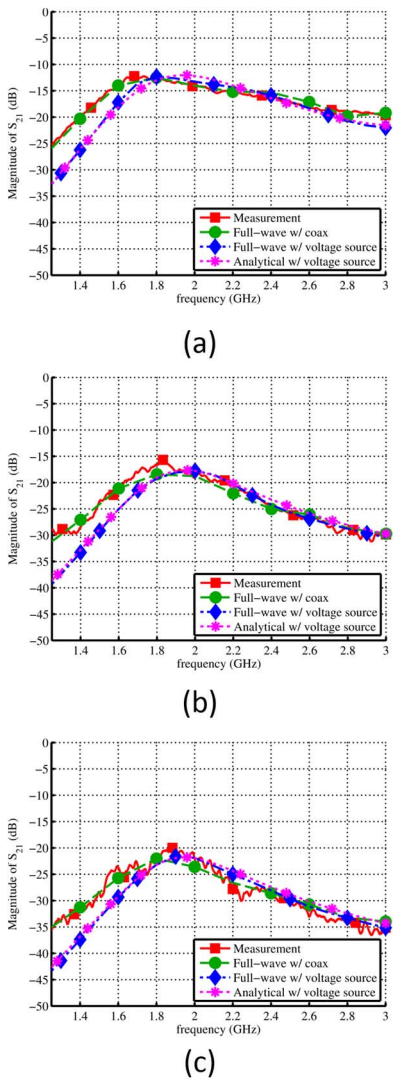

Fig. 14. Comparison of pseudo-analytical, full-wave (with and without coax) and measured S_{21} for copper loops separated by a distance of (a) $4b$, (b) $8b$ and (c) $12b$.

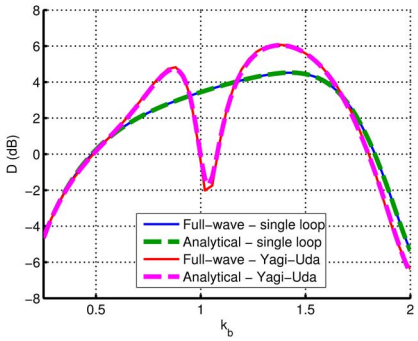

Fig. 15. Comparison of full-wave and analytical directivity versus k_b for a single loop and a Yagi–Uda array with a single reflector.

and the MIMO system capacity [36]. To showcase the practical impact of these analytical expressions, the directivity of two PEC loops with thickness factor $\Omega = 12$ in a stacked Yagi–Uda configuration will be considered. The passive

element is placed at a distance 0.5λ at $k_b = 1$ below the active element and has a radius 1.1 times larger than that of the active element. Fig. 15 shows a comparison of the full-wave and analytical directivity versus k_b for both the single loop and the Yagi–Uda array. As can be seen, the results are nearly identical. In addition, the full-wave simulation took 19 min to run with the thin-wire method of moments formulation while the analytical MATLAB code took only 89 s. Note that the directivity reaches the superdirective limit (6 dBi for a two-element array [37]) at a value of around $k_b = 1.37$.

IV. Conclusion

This paper presented two efficient methods of computing the mutual coupling between circular loop antennas: an exact pseudo-analytical approach and an approximate fully analytical expression. The approaches are valid in the terahertz, infrared, and optical regime when the effects of material dispersion and loss are taken into consideration. The commercial full-wave solver FEKO requires almost six hours to simulate the case of two lossy gold nanoloops, while the pseudo and fully analytical solutions as implemented in MATLAB require only 33 and 11 s, respectively. For the important special case of two loops in the stacked configuration, an extremely simple and efficient analytical expression was presented, which requires only 0.1 s to evaluate in MATLAB. Using these expressions, studies of the mutual admittance versus interelement spacing for any geometrical configuration and nanoloop material can easily and rapidly be performed. In addition, full mutual admittance matrices and the resulting radiation properties for an array of loops can be efficiently calculated. Mutual coupling is a crucial parameter which must be considered in the design of communication systems, MIMO and diversity systems, phased arrays, and energy harvesting devices. Due to its fundamental theoretical importance, its utility and ease of manufacture, the circular loop is among the most popular antennas for implementation in such systems. The pseudo-analytical (near-field) and fully analytical (far-field) expressions derived in this paper reduce the design cycle times of these systems from hours to seconds and provide the engineer with more physical insight.

Appendix A
Derivation of the Induced Current for the General Case

The expression in (27) can be derived by first applying the far-field approximations ($x = x_0, y = y_0, z = z_0, r = r_0, \rho = \rho_0$) to (11), which yields

$$\begin{aligned}\hat{r}\cdot\hat{t} &= \frac{\rho_0}{r_0}\sin(\phi_0-\phi')\\ \hat{\theta}\cdot\hat{t} &= \frac{z_0}{r_0}\sin(\phi_0-\phi')\\ \hat{\phi}\cdot\hat{t} &= \frac{1}{\rho_0}(\rho_0\cos(\phi_0-\phi')+b_j).\end{aligned} \tag{A.1}$$

After applying the appropriate far-field approximations, the θ-component of the induced current can be expressed in the form

$$\begin{aligned}I_{\theta,j}(\Phi') = -\frac{\eta_0 b_j z_0^2}{2\rho_0 r_0^2}e^{-jk_0r_0}\sum_{p=0}^{\infty}Y'_{p,j}\cdot\sum_{n=1}^{\infty}n(-j)^n I_{n,i}\\ \times J_n\left(\frac{k_0 b_i\rho_0}{r_0}\right)\sin(n\phi_0)\cdot\int_0^{2\pi}e^{-j\frac{k_0 b_j\rho_0}{r_0}\cos(\phi_0-\phi')}\\ \times\sin(\phi_0-\phi')\cos(p(\Phi'-\phi'))d\phi'.\end{aligned} \tag{A.2}$$

The sine and cosine functions can be written as complex exponentials such that the integrand in (A2) becomes

$$\begin{aligned}I_{\theta,j}(\Phi') = -\frac{\eta_0 b_j z_0^2}{8j\rho_0 r_0^2}e^{-jk_0r_0}\sum_{p=0}^{\infty}Y_{p,j}\\ \cdot\sum_{n=1}^{\infty}n(-j)^n I_{n,i}J_n\left(\frac{k_0 b_i\rho_0}{r_0}\right)\sin(n\phi_0)\\ \cdot\int_0^{2\pi}e^{-j\frac{k_0 b_j\rho_0}{r_0}\cos(\phi_0-\phi')}\\ \times[e^{j(p\Phi'+\phi_0)}e^{-j(p+1)\phi'}+e^{-j(p\Phi'-\phi_0)}e^{j(p-1)\phi'}\\ -e^{j(p\Phi'-\phi_0)}e^{-j(p-1)\phi'}\\ -e^{-j(p\Phi'+\phi_0)}e^{j(p+1)\phi'}]d\phi'.\end{aligned} \tag{A.3}$$

To solve the integral in (A3), it is convenient at this point to employ the Bessel generating function [31]

$$e^{\frac{x}{2}(t-\frac{1}{t})} = \sum_{k=-\infty}^{\infty}J_k(x)t^k,\quad t\neq 0. \tag{A.4}$$

Letting $x = (k_0 b_j\rho_0/r_0)$ and $t = -je^{j(\phi_0-\phi')}$ the first term in the integrand of (A3) can be represented as

$$e^{-j\frac{k_0 b_j\rho_0}{r_0}\cos(\phi_0-\phi')} = \sum_{k=-\infty}^{\infty}J_k\left(\frac{k_0 b_j\rho_0}{r_0}\right)(-j)^k e^{jk(\phi_0-\phi')}. \tag{A.5}$$

Substituting (A5) into (A3) and exploiting the fact that

$$\int_0^{2\pi}e^{jp\phi'}d\phi' = \begin{cases}0, & p\neq 0\\ 2\pi, & p=0\end{cases} \tag{A.6}$$

results in the following analytical expression:

$$\begin{aligned}I_{\theta,j}(\Phi') = -\frac{\pi\eta_0 b_j z_0^2}{4j\rho_0 r_0^2}e^{-jk_0r_0}\sum_{p=0}^{\infty}Y'_{p,j}\cdot\sum_{n=1}^{\infty}nj^n I_{n,i}\\ \times J_n\left(\frac{k_0 b_i\rho_0}{r_0}\right)\sin(n\phi_0)\\ \cdot\left[(-j)^{-p-1}J_{-p-1}\left(\frac{k_0 b_j\rho_0}{r_0}\right)e^{jp(\Phi'-\phi_0)}\right.\\ +(-j)^{p-1}J_{p-1}\left(\frac{k_0 b_j\rho_0}{r_0}\right)e^{-jp(\Phi'-\phi_0)}\\ -(-j)^{-p+1}J_{-p+1}\left(\frac{k_0 b_j\rho_0}{r_0}\right)e^{jp(\Phi'-\phi_0)}\\ \left.-(-j)^{p+1}J_{p+1}\left(\frac{k_0 b_j\rho_0}{r_0}\right)e^{-jp(\Phi'-\phi_0)}\right].\end{aligned} \tag{A.7}$$

Now by applying Euler's identity along with

$$J_{-m}(x) = (-1)^m J_m(x) \tag{A.8}$$

$$J_{m-1}(x) + J_{m+1}(x) = \frac{2m}{x} J_m(x) \tag{A.9}$$

the expression in (A7) can be simplified to

$$\begin{aligned} &I_{\theta,j}(\Phi') \\ &= -\frac{\pi \eta_0 z_0^2}{\rho_0^2 r_0 k_0} e^{-jk_0 r_0} \sum_{p=0}^{\infty} Y'_{p,j} \cdot \sum_{n=1}^{\infty} n j^n I_{n,i} J_n\left(\frac{k_0 b_i \rho_0}{r_0}\right) \sin(n\phi_0) \\ &\quad \times \left[j^{p-1}(-1)^p \sin(p(\Phi' - \phi_0)) p J_p\left(\frac{k_0 b_j \rho_0}{r_0}\right)\right]. \end{aligned} \tag{A.10}$$

Similarly, the ϕ-component of the induced current is given by

$$\begin{aligned} &I_{\phi,j}(\Phi') \\ &= -\frac{\eta_0 k_0 b_i b_j}{2r_0} e^{-jk_0 r_0} \sum_{p=0}^{\infty} Y'_{p,j} \cdot \sum_{n=0}^{\infty} j^n I_{n,i} J'_n\left(\frac{k_0 b_i \rho_0}{r_0}\right) \\ &\quad \times \cos(n\phi_0) \int_0^{2\pi} \left[\frac{b_j}{\rho_0} + \cos(\phi_0 - \phi')\right] \\ &\quad \times e^{-j\frac{k_0 b_j \rho_0}{r_0}\cos(\phi_0 - \phi')} \cdot \cos(p(\Phi' - \phi_0)) d\phi'. \end{aligned} \tag{A.11}$$

The preceding integral can be split into two separate integrals and evaluated individually, where

$$\begin{aligned} I_{\phi 1,j}(\Phi') &= -\frac{\eta_0 k_0 b_i b_j^2}{2r_0 \rho_0} e^{-jk_0 r_0} \sum_{p=0}^{\infty} Y'_{p,j} \\ &\quad \cdot \sum_{n=0}^{\infty} j^n I_{n,i} J'_n\left(\frac{k_0 b_i \rho_0}{r_0}\right) \cos(n\phi_0) \\ &\quad \cdot \int_0^{2\pi} e^{-j\frac{k_0 b_j \rho_0}{r_0}\cos(\phi_0 - \phi')} \cos(p(\Phi' - \phi')) d\phi' \end{aligned} \tag{A.12}$$

$$\begin{aligned} I_{\phi 2,j}(\Phi') &= -\frac{\eta_0 k_0 b_i b_j}{2r_0} e^{-jk_0 r_0} \sum_{p=0}^{\infty} Y'_{p,j} \\ &\quad \cdot \sum_{n=0}^{\infty} j^n I_{n,i} J'_n\left(\frac{k_0 b_i \rho_0}{r_0}\right) \cos(n\phi_0) \\ &\quad \cdot \int_0^{2\pi} e^{-j\frac{k_0 b_j \rho_0}{r_0}\cos(\phi_0 - \phi')} \\ &\quad \times \cos(\phi_0 - \phi') \cos(p(\Phi' - \phi')) d\phi'. \end{aligned} \tag{A.13}$$

After applying (A5), Euler's identity, (A6) and (A8), the expression in (A12) reduces to

$$\begin{aligned} I_{\phi 1,j}(\Phi') &= -\frac{\pi \eta_0 k_0 b_i b_j^2}{\rho_0 r_0} e^{-jk_0 r_0} \sum_{p=0}^{\infty} Y'_{p,j} \\ &\quad \cdot \sum_{n=0}^{\infty} j^n I_{n,i} J'_n\left(\frac{k_0 b_i \rho_0}{r_0}\right) \cos(n\phi_0) \\ &\quad \times \left[(-j)^p J_p\left(\frac{k_0 b_j \rho_0}{r_0}\right) \cos(p(\Phi' - \phi_0))\right]. \end{aligned} \tag{A.14}$$

Similarly, by using (A5) and (A6), the expression in (A13) becomes

$$\begin{aligned} &I_{\phi 2,j}(\Phi') \\ &= -\frac{\pi \eta_0 k_0 b_i b_j}{4r_0} e^{-jk_0 r_0} \sum_{p=0}^{\infty} Y'_{p,j} \cdot \sum_{n=0}^{\infty} j^n I_{n,i} \\ &\quad \times J'_n\left(\frac{k_0 b_i \rho_0}{r_0}\right) \cos(n\phi_0) \\ &\quad \cdot \left[(-j)^{-p-1} J_{-p-1}\left(\frac{k_0 b_j \rho_0}{r_0}\right) e^{jp(\Phi' - \phi_0)}\right. \\ &\quad + (-j)^{p-1} J_{p-1}\left(\frac{k_0 b_j \rho_0}{r_0}\right) e^{-jp(\Phi' - \phi_0)} \\ &\quad + (-j)^{-p+1} J_{-p+1}\left(\frac{k_0 b_j \rho_0}{r_0}\right) e^{jp(\Phi' - \phi_0)} \\ &\quad \left. + (-j)^{p+1} J_{p+1}\left(\frac{k_0 b_j \rho_0}{r_0}\right) e^{-jp(\Phi' - \phi_0)}\right]. \end{aligned} \tag{A.15}$$

Next, by using Euler's identity in conjunction with (A8) and

$$J_{m-1}(x) - J_{m+1}(x) = 2J'_m(x) \tag{A.16}$$

the expression in (A15) can be reduced to

$$\begin{aligned} &I_{\phi 2,j}(\Phi') \\ &= -\frac{\pi \eta_0 k_0 b_i b_j}{r_0} e^{-jk_0 r_0} \sum_{p=0}^{\infty} Y'_{p,j} \\ &\quad \cdot \sum_{n=0}^{\infty} j^n I_{n,i} J'_n\left(\frac{k_0 b_i \rho_0}{r_0}\right) \cos(n\phi_0) \\ &\quad \times \cos(p(\Phi' - \phi_0))(-j)^{p-1} J'_p\left(\frac{k_0 b_j \rho_0}{r_0}\right). \end{aligned} \tag{A.17}$$

Then, the expression for the ϕ-component of the induced current can be determined by adding (A14) and (A17)

$$\begin{aligned} &I_{\phi,j}(\Phi') \\ &= -\frac{\pi \eta_0 k_0 b_i b_j}{r_0} e^{-jk_0 r_0} \sum_{p=0}^{\infty} Y'_{p,j} \\ &\quad \sum_{n=0}^{\infty} I_{n,i} J'_n\left(\frac{k_0 b_i \rho_0}{r_0}\right) \cos(n\phi_0) \\ &\quad \times \left[\frac{b_j}{\rho_0}(-1)^p j^{n+p} J_p\left(\frac{k_0 b_j \rho_0}{r_0}\right) + (-1)^{p-1}\right. \\ &\quad \left. \times j^{n+p-1} J'_p\left(\frac{k_0 b_j \rho_0}{r_0}\right)\right] \cos(p(\Phi' - \phi_0)). \end{aligned} \tag{A.18}$$

Finally, the radial component of the near-zone electric field given in (11) can be simplified using (25) and (26)

$$\begin{aligned} E_r(r,\theta,\phi) &= \frac{\eta_0 b_i \sin\theta_0}{4r_0^2} \sum_{m=1}^{\infty} \sum_{\substack{n=1 \\ m-n=2k \\ k=0,1,\ldots}}^{m} \left(\frac{k_0 b_i \sin\theta_0}{2}\right)^{m-1} \\ &\quad \cdot \sin(n\phi_0) j^{m+1} e^{-jk_0 r} \left[j\frac{k_0 b_i^2}{r_0} C^3_{\mathrm{mn},i} - C^4_{\mathrm{mn},i}\right]. \end{aligned} \tag{A.19}$$

Next, we consider taking the dot product between $\hat{r}$ and $b_j\hat{t}$ which yields

$$b_j\hat{r}\cdot\hat{t} = \frac{b_j\rho_0^2}{r_0}\sin(\phi_0-\phi'). \tag{A.20}$$

Hence, the r-component of the induced current may be represented as

$$\begin{aligned} I_{r,j}(\Phi') = {} & \frac{\eta_0 b_i b_j \rho_0^2}{4r_0^4}\sum_{m=1}^{\infty}\sum_{\substack{n=1\\ m-n=2k\\ k=0,1,\ldots}}^{m}\left(\frac{k_0 b_i\sin\theta_0}{2}\right)^{m-1}\sin(n\phi_0) \\ & \cdot j^{m+1}e^{-jk_0r_0}\left[\frac{jk_0b_i^2}{r_0}C^3_{\mathrm{mn},i}-C^4_{\mathrm{mn},i}\right] \\ & \cdot\sum_{p=0}^{\infty}Y'_{p,j}\int_0^{2\pi}e^{-j\frac{k_0b_j\rho_0}{r_0}\cos(\phi_0-\phi')} \\ & \cdot\sin(\phi_0-\phi')\cos(p(\Phi'-\phi'))d\phi' \end{aligned} \tag{A.21}$$

where the integral is identical to that calculated for the $I_{\theta,j}$ term in (A2). Following the same procedure, the r-component of the induced current can be simplified to

$$\begin{aligned} & I_{r,j}(\Phi') \\ & = \frac{\pi\eta_0 b_i\rho_0}{2r_0^3k_0}e^{-jk_0r_0}\sum_{m=1}^{\infty}\sum_{\substack{n=1\\ m-n=2k\\ k=0,1,\ldots}}^{m}\left(\frac{k_0b_i\sin\theta_0}{2}\right)^{m-1} \\ & \quad\times\sin(n\phi_0)\cdot j^{m+1}\left[\frac{jk_0b_i^2}{r_0}C^3_{\mathrm{mn},i}-C^4_{\mathrm{mn},i}\right] \\ & \quad\cdot\sum_{p=0}^{\infty}Y'_{p,j}\,p(-1)^p j^{p-1}\sin(p(\Phi'-\phi_0))J_p\left(\frac{k_0b_j\rho_0}{r_0}\right). \end{aligned} \tag{A.22}$$

The total induced current is the sum of (A10), (A18), and (A22).

Appendix B
Derivation of the Induced Current for the Stacked Loop Case

For the stacked loop case, $\rho_0 = 0$, $\rho = b_j$, $r_0 = z_0$, and $r = (b_j^2+z_0^2)^{1/2}$. Since $\hat{\theta}\cdot\hat{t}$ and $\hat{r}\cdot\hat{t}$ are both zero, and $\hat{\phi}\cdot b_j\hat{t} = b_j$, only the ϕ-component of the induced current is nonzero

$$\begin{aligned} I_{\phi,j}(\Phi') = {} & -\frac{\eta_0k_0b_ib_j}{2r}e^{-jk_0r}\sum_{n=0}^{\infty}j^nI_{n,i}J'_n\left(\frac{k_0b_ib_j}{r}\right) \\ & \cdot\sum_{p=0}^{\infty}Y'_{p,j}\int_0^{2\pi}\cos(n\phi')\cos(p(\Phi'-\phi'))d\phi' \end{aligned} \tag{B.1}$$

where $\sin\theta = \frac{b_j}{r}$ has been applied. This expression can be rewritten using Euler's identity

$$\begin{aligned} & I_{\phi,j}(\Phi') \\ & = -\frac{\eta_0k_0b_ib_j}{8r}e^{-jk_0r}\sum_{n=0}^{\infty}j^nI_{n,i}J'_n\left(\frac{k_0b_ib_j}{r}\right)\cdot\sum_{p=0}^{\infty}Y'_{p,j} \\ & \quad\times\left[e^{jp\Phi'}\int_0^{2\pi}e^{j(n-p)\phi'}d\phi'\right. \\ & \quad + e^{-jp\Phi'}\int_0^{2\pi}e^{j(n+p)\phi'}d\phi' + e^{jp\Phi'} \\ & \quad\times\int_0^{2\pi}e^{-j(n+p)\phi'}d\phi' \\ & \quad\left. + e^{-jp\Phi'}\int_0^{2\pi}e^{-j(n-p)\phi'}d\phi'\right]. \end{aligned} \tag{B.2}$$

Using (A6), (B2) has nonzero terms only when $n = p = 0, 1, 2\ldots$ or $n = -p = 0$. Employing the Bessel generating function results in the analytical expression (27), reproduced here for convenience

$$\begin{aligned} I_{\phi,j}(\Phi') = {} & -\frac{\pi\eta_0k_0b_ib_j}{2r}e^{-jk_0r} \\ & \cdot\left[\sum_{p=0}^{\infty}j^pI_{p,i}Y_{p,j}J'_p\left(\frac{k_0b_ib_j}{r}\right)\cos(p\Phi')\right. \\ & \left. + I_{0,i}Y_{0,j}J'_0\left(\frac{k_0b_ib_j}{r}\right)\right]. \end{aligned} \tag{B.3}$$

Acknowledgment

The authors would like to thank Dr. J. Roe for his insightful mathematical discussions on coordinate transformation problems related to this paper.

References

[1] G. S. Smith, "Loop antennas," in *Antenna Engineering Handbook*, R. Johnson, Ed. New York, NY, USA: McGraw-Hill, 1993.
[2] D. G. Large, L. Ball, and A. Farstad, "Radio transmission to and from underground coal mines–theory and measurement," *IEEE Trans. Commun.*, vol. COM-21, no. 3, pp. 194–202, Mar. 1973.
[3] J. A. Fuller and J. R. Wait, "Mutual electromagnetic coupling of coaxial loops in a borehole," *Radio Sci.*, vol. 8, no. 5, pp. 453–457, May 1973.
[4] R. L. Yadava, *Antenna and Wave Propagation*. New Delhi, India: Phi Learning Private Limited, 2011.
[5] J. Schulte, Ed., *Nanotechnology: Global Strategies, Industry Trends and Applications*. Chichester, U.K.: Wiley, 2005.
[6] P. Biagioni, J.-S. Huang, and B. Hecht, "Nanoantennas for visible and infrared radiation," *Rep. Prog. Phys.*, vol. 75, pp. 024402-1–024402-40, Jan. 2012.
[7] C. A. Balanis, *Antenna Theory*. New York, NY, USA: Wiley, 1997.
[8] R. Zhou, J. Ding, B. Arigong, Y. Lin, and H. Zhang, "Design of a new broadband monopole optical nano-antenna," *J. Appl. Phys.*, vol. 114, no. 18, pp. 184305-1–184305-5, 2013.
[9] F. P. G. de Arquer, V. Volski, N. Verellen, G. A. E. Vandenbosch, and V. V. Moshchalkov, "Engineering the input impedance of optical nano dipole antennas: Materials, geometry and excitation effect," *IEEE Trans. Antennas Propag.*, vol. 59, no. 9, pp. 3144–3153, Sep. 2011.
[10] P. J. Schuck, D. P. Fromm, A. Sundaramurthy, G. S. Kino, and W. E. Moerner, "Improving the mismatch between light and nanoscale objects with gold bowtie nanoantennas," *Phys. Rev. Lett.*, vol. 94, pp. 1–4, Jan. 2005.

[11] M. Alavirad, L. Roy, and P. Berini, "Optimization of plasmonic nanodipole antenna arrays for sensing applications," *IEEE J. Sel. Topics Quantum Electron.*, vol. 20, no. 3, pp. 4600308-1–4600308-8, Apr. 2014.
[12] H. Chen, A. M. Bhuiya, R. Liu, D. M. Wasserman, and K. C. Toussaint, "Design, fabrication, and characterization of near-IR gold bowtie nanoantenna arrays," *J. Phys. Chem.*, vol. 118, pp. 20553–20558, Aug. 2014.
[13] A. F. McKinley, T. P. White, and K. R. Catchpole, "Theory of the circular closed loop antenna in the terahertz, infrared, and optical regions," *J. Appl. Phys.*, vol. 114, pp. 044317-1–044317-10, Jul. 2013.
[14] C. Simovski, D. Morits, P. Voroshilov, M. Guzhva, P. Belov, and Y. Kivshar, "Enhanced efficiency of light-trapping nanoantenna arrays for thin-film solar cells," *Opt. Exp.*, vol. 21, no. S4, pp. A714–A725, 2013.
[15] A. F. McKinley, T. P. White, and K. R. Catchpole, "Designing nanoloop antenna arrays for light-trapping in solar cells," in *Proc. Photovolt. Specialists Conf. (PVSC)*, 2013, pp. 1894–1896.
[16] A. Ahmadi and H. Mosallaei, "Plasmonic nanoloop array antenna," *Opt. Lett.*, vol. 35, pp. 3706–3708, Sep. 2010.
[17] J. E. Storer, "Impedance of thin-wire loop antennas," *Trans. Amer. Inst. Electr. Eng., I, Commun. Electron.*, vol. 75, no. 5, pp. 606–619, Nov. 1956.
[18] T. T. Wu, "Theory of the thin circular loop antenna," *J. Math. Phys.*, vol. 3, no. 6, pp. 1301–1304, Nov./Dec. 1962.
[19] A. F. McKinley, T. P. White, I. S. Maksymov, and K. R. Catchpole, "The analytical basis for the resonances and anti-resonances of loop antennas and meta-material ring resonators," *J. Appl. Phys.*, vol. 112, pp. 094911-1–094911-9, Aug. 2012.
[20] D. H. Werner, "An exact integration procedure for vector potentials of thin circular loop antennas," *IEEE Trans. Antennas Propag.*, vol. 44, no. 2, pp. 157–165, Feb. 1996.
[21] D. H. Werner, "Lommel expansions in electromagnetics," in *Frontiers in Electromagnetics*, D. H. Werner and R. Mittra, Eds. Hoboken, NJ, USA: Wiley, 2000.
[22] B. Q. Lu, J. Nagar, T. Yue, M. F. Pantoja, and D. H. Werner, "Closed-form expressions for the radiation properties of nanoloops in the terahertz, infrared and optical regimes," *IEEE Trans. Antennas Propag.*, vol. 64, no. 12, pp. 121–133, Dec. 2016.
[23] R. Hansen, "Formulation of echelon dipole mutual impedance for computer," *IEEE Trans. Antennas Propag.*, vol. 20, no. 6, pp. 780–781, Nov. 1972.
[24] S. S. Kakatkar and K. P. Ray, "Evaluation of mutual coupling between slots from dipole expressions," *Prog. Electromagn. Res. M*, vol. 9, pp. 123–138, 2009.
[25] K. Iizuka, R. W. P. King, and C. W. Harrison, "Self- and mutual admittances of two identical circular loop antennas in a conducting medium and in air," *IEEE Trans. Antennas Propag.*, vol. AP-14, no. 4, pp. 440–450, Apr. 1966.
[26] S. Ito, N. Inagaki, and T. Sekiguchi, "An investigation of the array of circular-loop antennas," *IEEE Trans. Antennas Propag.*, vol. AP-19, no. 4, pp. 469–476, Jul. 1971.
[27] J. R. Wait, "Mutual electromagnetic coupling of loops over a homogeneous ground," *Soc. Exploration Geophys.*, vol. 20, no. 3, pp. 630–637, 1955.
[28] J. A. Fuller and J. R. Wait, "High-frequency electromagnetic coupling between small coplanar loops over an inhomogeneous ground," *Soc. Exploration Geophys.*, vol. 37, no. 6, pp. 997–1004, 1972.
[29] S. Krishnan, L. W. Li, and M. S. Leong, "Entire-domain MoM analysis of an array of arbitrary oriented circular loop antennas: A general formulation," *IEEE Trans. Antennas Propag.*, vol. 53, no. 9, pp. 2961–2968, Sep. 2005.
[30] *FEKO Suite 7.0, EM Software & Systems—S. A., Stellenbosch, South Africa*. Accessed: Sep. 17, 2017. [Online]. Available: http://www.feko.info
[31] P. B. Johnson and R. W. Christy, "Optical constants of the noble metals," *Phys. Rev. B, Condens. Matter*, vol. 6, no. 12, pp. 4370–4379, Dec. 1972.
[32] L. Novotny and B. Hecht, *Principles of Nano-Optics*. Cambridge, U.K.: Cambridge Univ. Press, 2012.
[33] L. F. Shampine, "Vectorized adaptive quadrature in MATLAB," *J. Comput. Appl. Math.*, vol. 211, pp. 131–140, Apr. 2008.
[34] M. Abramowitz and I. Stegun, *Handbook of Mathematical Functions With Formulas, Graphs, and Mathematical Tables*. New York, NY, USA: Dover, 1964.
[35] D. E. Amos, "A portable package for Bessel functions of a complex argument and nonnegative order," *Trans. Math. Softw.*, vol. 12, no. 3, pp. 265–273, 1986.
[36] H. Singh, H. Sneha, and R. Jha, "Mutual coupling in phased arrays: A review," *Int. J. Antennas Propag.*, vol. 2013, pp. 1–23, 2013.
[37] A. Haskou, A. Sharaiha, and S. Collardey, "Theoretical and practical limits of superdirective antenna arrays," *Comp. Rendus Phys.*, vol. 18, no. 2, pp. 118–124.

Jogender Nagar (S'09) received the B.S. degree in electrical and computer engineering from the Ohio State University, Columbus, OH, USA, in 2008, and the M.S. degree in electrical engineering from Johns Hopkins University, Baltimore, MD, USA, in 2011.

He was with Northrop Grumman, Baltimore, MD, USA, for two years. He is a member of the Computational Electromagnetics and Antennas Research Lab, Pennsylvania State University, State College, PA, USA. His current research interests include computational electromagnetics, antenna theory and design, transformation optics, gradient-index lens design, multi-objective optimization, and nanoantennas.

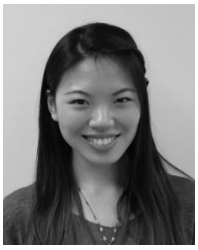

Bing Qian Lu (S'14) received the B.S. degree in mathematics and the M.S. degree in electrical engineering from the Pennsylvania State University, State College, PA, USA, in 2014 and 2016, respectively.

Her current research interests include applied electromagnetics, antenna engineering, metamaterials, plasmonic antennas, and transformation optics.

Mario F. Pantoja (M'97–SM'12) received the B.S., M.S., and Ph.D. degrees in electrical engineering from the University of Granada, Granada, Spain, in 1996, 1998, and 2001, respectively.

Since 2004, he has been an Associate Professor with the University of Granada. He has authored more than 50 refereed journal articles and book chapters, and more than 100 conference papers and technical reports, and he has participated in more than 40 national and international projects with public and private funding. His current research interests include the areas of time-domain analysis of electromagnetic radiation and scattering problems, optimization methods applied to antenna design, Terahertz technology, and nanoelectromagnetics.

Dr. Pantoja was a recipient of a 2002 International Union of Radio Science Young Scientist Award. He was a Visiting Scholar with the Dipartimento Ingenieria dell'Informazione, University of Pisa, Pisa, Italy; the International Research Centre for Telecommunications and Radar, Delft University of Technology, Delft, The Netherlands; and the Antenna and Electromagnetics Group, Denmark Technical University, Kongens Lyngby, Denmark. In addition, he has received a Fulbright Grant to collaborate with the Computational Electromagnetics and Antenna Research Laboratory at the Pennsylvania State University, State College, PA, USA.

Douglas H. Werner (F'05) received the B.S., M.S., and Ph.D. degrees in electrical engineering and the M.A. degree in mathematics from the Pennsylvania State University (Penn State), University Park, PA, USA, in 1983, 1985, 1989, and 1986, respectively.

He holds the John L. and Genevieve H. McCain Chair Professorship with the Department of Electrical Engineering, Penn State. He is the Director of the Computational Electromagnetics and Antennas Research Lab, a member of the Communications and Space Sciences Lab, and also a Faculty Member of the Materials Research Institute with Penn State. He has authored over 750 technical papers and proceedings articles, 25 book chapters with several additional chapters currently in preparation, and holds 13 patents. He has authored several books including *Frontiers in Electromagnetics* (IEEE Press, 2000), *Genetic Algorithms in Electromagnetics* (Wiley/IEEE, 2007), *Transformation Electromagnetics and Metamaterials: Fundamental Principles and Applications* (Springer, 2014), and *Electromagnetics of Body Area Networks: Antennas, Propagation, and RF Systems* (Wiley/IEEE, 2016). He has co-authored (with one of his graduate students) a paper published in the IEEE TRANSACTIONS ON ANTENNAS AND PROPAGATION which received the 2006 R. W. P. King Award. He has also contributed chapters for several books including *Electromagnetic Optimization by Genetic Algorithms* (Wiley Interscience, 1999), *Soft Computing in Communications* (Springer, 2004), *Antenna Engineering Handbook* (McGraw-Hill, 2007), *Frontiers in Antennas: Next Generation Design and Engineering* (McGraw-Hill, 2011), *Numerical Methods for Metamaterial Design* (Springer, 2013), *Computational Electromagnetics* (Springer, 2014), *Graphene Science Handbook: Nanostructure and Atomic Arrangement* (CRC Press, 2016), and *Handbook of Antenna Technologies* (Springer, 2016). His current research interests include computational electromagnetics, antenna theory and design, phased arrays (including ultra-wideband arrays), microwave devices, wireless and personal communication systems (including on-body networks), wearable and e-textile antennas, RFID tag antennas, conformal antennas, reconfigurable antennas, frequency selective surfaces, electromagnetic wave interactions with complex media, metamaterials, electromagnetic bandgap materials, zero and negative index materials, transformation optics, nanoscale electromagnetics (including nanoantennas), fractal and knot electrodynamics, and nature-inspired optimization techniques (genetic algorithms, clonal selection algorithms, particle swarm, wind driven optimization, and various other evolutionary programming schemes).

Prof. Werner is a Fellow of the IET (formerly IEE), the OSA and the ACES and a member of URSI Commissions B and G, Eta Kappa Nu, Tau Beta Pi and Sigma Xi. He was a recipient of the 1993 Applied Computational Electromagnetics Society Best Paper Award, a 1993 International Union of Radio Science Young Scientist Award, and the Pennsylvania State University Applied Research Laboratory Outstanding Publication Award in 1994, the inaugural IEEE Antennas and Propagation Society Edward E. Altshuler Prize Paper Award and the Harold A. Wheeler Applications Prize Paper Award in 2011 and 2014, respectively, the 2015 ACES Technical Achievement Award, a College of Engineering PSES Outstanding Research Award and Outstanding Teaching Award in 2000 and 2002, respectively, the IEEE Central Pennsylvania Section Millennium Medal and the PSES Premier Research Award in 2009. He is a Former Associate Editor of *Radio Science*, a former Editor of the *IEEE Antennas and Propagation Magazine*, an Associate Editor of the Nature subjournal *Scientific Reports*.